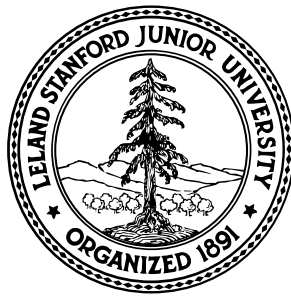


A theory for the subfilter-scale model in large-eddy simulation

Fotini V. Katopodes, Robert L. Street, Joel H. Ferziger

March, 2000



Technical Report 2000-K1

Environmental Fluid Mechanics Laboratory
Stanford, CA 94305-4020

© Copyright by Fotini V. Katopodes 2000
All rights reserved.

Abstract

A new subfilter-scale (SFS) stress model for large-eddy simulation (LES) is proposed using successive inversion of a Taylor series expansion to represent the unknown full velocity in terms of the filtered velocity. The resulting expression for the SFS stress satisfies the SFS stress evolution equations to a predefined order of accuracy in the filter width (the truncation order of the series expansion). The modeled SFS stress is thus influenced by buoyancy, viscous, pressure, and Coriolis effects just as the velocity field is. The series expansion model is of scale-similarity form, and reduces to the Bardina model [1] at lowest order. Preliminary tests of the model are presented using a modified wave number analysis and *a priori* testing using a direct numerical simulation (DNS) of sheared, stably-stratified homogeneous turbulence. It is found that the model exhibits very high correlations with the exact SFS stress.

Introduction

Large-eddy simulation is a method in which the larger scales of a turbulent flow are simulated accurately, while the smaller, subfilter, scales are not resolved in the numerical simulation and must be modeled. (We use the term “subfilter-scale”, rather than “subgrid-scale”, to denote the unresolved velocity and stress fields, as the size of the filter should be greater than the size of the grid upon which spatial discretization is based [2].) The subfilter-scale model must be based on knowledge of the resolved scale behavior alone. Leonard [3] provided early theoretical and practical bases for LES. Bardina *et al.* [1] made a seminal contribution by introducing the scale-similarity model, which has been shown to be an essential component of a correct SFS model. While eddy viscosity models such as that used by Smagorinsky [4] assume a form for the SFS stress, scale-similarity models create an approximation to the full velocity field and use this to estimate the SFS stress, $\tau_{ij} = \overline{u_i u_j} - \overline{u_i} \overline{u_j}$. Thus, in the Bardina model, the full velocity is approximated by the filtered velocity, $u_i \approx \overline{u_i}$, to obtain $\tau_{ij} \approx \overline{\overline{u_i} \overline{u_j}} - \overline{\overline{u_i}} \overline{\overline{u_j}}$. This was the first SFS model that used the smallest resolved scales as its basis.

Further improvement in estimates of the SFS stress were seen with the introduction of dynamic models. Zang *et al.* [5] introduced a two-component model based on Bardina’s mixed model [1] and the dynamic model of Germano *et al.* [6]. Mixed models can represent both back-scatter of small-scale energy to the larger scales and forward-scatter, or dissipation of large-scale energy by the small scales; both are essential for a reasonable representation of the subfilter-scale effects. Piomelli [7], Sarghini *et al.* [8], and Lesieur and Métais [9] give comprehensive reviews of and further insights to large-eddy simulation and the variety of subfilter-scale models that have been introduced.

In the scale-similarity approach, the approximation for τ_{ij} would be more accurate if a higher order approximation to the full velocity field could be obtained. A more exact representation of SFS motions is especially desirable for applications of LES to computation of complex flows, including geophysical flows. In such cases the subfilter scales are probably not isotropic, as assumed in eddy viscosity SFS models. Shah and Ferziger [10] proposed a new non-eddy-viscosity model (the stimulated small scale, or S^3 , model) in which a local approximation of total quantities in terms of filtered ones is introduced; the scale-similarity model is a special case. In this paper we propose a simplified version of the S^3 model.

Domaradzki and Saiki [11] also developed a method which creates an estimate of the subfilter-scale velocity based on the resolved scales. This estimate is then used to calculate the SFS stress. Their model is a generalization of Bardina’s scale-similarity model. The model was designed for spectral space calculations, but has been extended to physical space by Domaradzki and Loh [12]. With a similar approach, Geurts [13] developed a generalized scale-similarity model using a polynomial to approximate the inverse filtering operation. Recently, Stolz and Adams [14] also proposed an approximate deconvolution procedure for estimating the velocity.

Velocity estimation methods that lead to models of the scale-similarity type are only valid for flows in which the interaction between resolved and unresolved scales occurs primarily in the vicinity of the filter cutoff. As noted by Domaradzki and Saiki [11], this seems to be the case for all low Reynolds number cases that have been investigated experimentally and numerically (see *e.g.* [15]).

In the SFS model described here, the unresolved velocity is represented by successive inversion of a Taylor series expansion of the resolved velocity field. This representation is used to estimate the velocity in the same spirit as the recently introduced methods described above. The expansion is easily derived and can be shown to be a good approximation to the

unresolved velocity field, at least in low Reynolds number flows. The mathematical expansion serves to close the Navier-Stokes equations by providing an expression for the subfilter stress, τ_{ij} . Furthermore, in analogy to Reynolds-averaged modeling where the Reynolds stress equations are modeled, one can derive the evolution equations for the subfilter-scale stress. These evolution equations allow systematic evaluation of the relative contributions by advection, diffusion, dissipation, pressure, rotation, and stratification in the subfilter-scale effects felt by the resolved components of the flow. The approach is similarly applied to the scalar transport equation, as done by Katopodes *et al.*[16].

In this paper, we prove that the model for the stresses obtained by the series expansion method is an *exact* solution of the evolution equations for the subfilter-scale stresses, to a known accuracy (the series truncation order) in the filter width. We subsequently illustrate the behavior of this model applied to a test function, and give results from *a priori* tests based on DNS data for a stably-stratified shear flow.

An important feature of the series model is that it is easily applied when the filter width is not equal in all directions, which is the case for the DNS data used herein. No parameters occur in the model, and nothing is assumed about the form of the SFS motions. The model should thus be able to capture anisotropic motions better than eddy viscosity models. Furthermore, the order of accuracy of the method is determined by the series truncation order chosen. Models of the scale-similar form are also invariant under Galilean transformations [17], and exhibit correct near-wall behavior [8]. The S^3 model of Shah and Ferziger [10], to which this model is related, has been shown to be superior to the Smagorinsky and mixed models in LES of plane channel flow and flow past a cubic obstacle [18]. Similar behavior is expected with the series expansion model as the two models are equivalent to fourth order in the filter width [19]. The model presented here is also very easy to implement.

Derivation of SFS evolution equations and series expansion model

In the following discussion, all variables are assumed to be smooth; no discretization is applied. We begin with the Navier-Stokes equations, written with the Boussinesq approximation for buoyancy effects and the Coriolis force included,

$$\frac{\partial u_i}{\partial t} + u_j \frac{\partial u_i}{\partial x_j} = -\frac{1}{\rho_0} \frac{\partial P}{\partial x_i} + \nu \frac{\partial^2 u_i}{\partial x_j \partial x_j} - \frac{\rho}{\rho_0} g \delta_{i3} + \epsilon_{imn} f_n u_m. \quad (1)$$

Here u_i denotes the velocity, ρ the density, ρ_0 the reference density, ν the kinematic viscosity, P the pressure, and f_n the Coriolis parameter. Repeated indices indicate summation. The spatially filtered equations are

$$\frac{\partial \bar{u}_i}{\partial t} + \bar{u}_j \frac{\partial \bar{u}_i}{\partial x_j} = -\frac{1}{\rho_0} \frac{\partial \bar{P}}{\partial x_i} + \nu \frac{\partial^2 \bar{u}_i}{\partial x_j \partial x_j} - \frac{\bar{\rho}}{\rho_0} g \delta_{i3} + \epsilon_{imn} f_n \bar{u}_m - \frac{\partial \tau_{ij}}{\partial x_j} \quad (2)$$

where the SFS stress is defined as

$$\tau_{ij} = \overline{u_i u_j} - \bar{u}_i \bar{u}_j. \quad (3)$$

Properties of the filter are described later. The filtered equations are not closed due to the nonlinear term $\overline{u_i u_j}$ included in τ_{ij} . We can seek to close the problem by developing an evolution equation for τ_{ij} by the following procedure.

We first obtain an evolution equation for $u_i u_k$ by multiplying the Navier-Stokes equation for u_i by u_k , the analogous equation for u_k by u_i , and adding the two equations together.

We then use integration by parts to express the viscous and pressure terms in more familiar forms. Filtering the resulting equation gives the evolution equation for $\overline{u_i u_k}$. Similarly, we can develop an evolution equation for $\overline{u_i} \overline{u_k}$. Now subtracting the equation for $\overline{u_i} \overline{u_k}$ from the equation for $\overline{u_i u_k}$, we obtain an evolution equation for τ_{ij} :

$$\begin{aligned}
\frac{\partial \tau_{ik}}{\partial t} + \overline{u_j} \frac{\partial \tau_{ik}}{\partial x_j} &= -\overline{u_j} \frac{\partial \overline{u_i u_k}}{\partial x_j} + \overline{u_j} \frac{\partial \overline{u_i} \overline{u_k}}{\partial x_j} + \overline{u_k} \frac{\partial \tau_{ij}}{\partial x_j} + \overline{u_i} \frac{\partial \tau_{kj}}{\partial x_j} \\
&- \frac{1}{\rho_0} \left(\frac{\partial \overline{u_i} \overline{P}}{\partial x_k} - \frac{\partial \overline{u_i} \overline{P}}{\partial x_k} + \frac{\partial \overline{u_k} \overline{P}}{\partial x_i} - \frac{\partial \overline{u_k} \overline{P}}{\partial x_i} \right) \\
&+ \frac{1}{\rho_0} \left(\overline{P} \frac{\partial u_i}{\partial x_k} - \overline{P} \frac{\partial \overline{u_i}}{\partial x_k} + \overline{P} \frac{\partial u_k}{\partial x_i} - \overline{P} \frac{\partial \overline{u_k}}{\partial x_i} \right) \\
&+ \nu \frac{\partial^2 \tau_{ik}}{\partial x_j \partial x_j} - 2\nu \frac{\partial \overline{u_i}}{\partial x_j} \frac{\partial \overline{u_k}}{\partial x_j} + 2\nu \frac{\partial \overline{u_i}}{\partial x_j} \frac{\partial \overline{u_k}}{\partial x_j} \\
&- \frac{g}{\rho_0} (\overline{\rho u_k} \delta_{i3} - \overline{\rho} \overline{u_k} \delta_{i3} + \overline{\rho u_i} \delta_{k3} - \overline{\rho} \overline{u_i} \delta_{k3}) \\
&+ f_n (\epsilon_{imn} \tau_{mk} - \epsilon_{kmn} \tau_{mi}) .
\end{aligned} \tag{4}$$

It has been assumed that the filtering operation commutes with the spatial derivatives, which is true for a spatially homogeneous filter. Some error is introduced if this is not so [20].

Equation (4) describes the evolution of the SFS stress tensor τ_{ik} ; it is seen that τ_{ik} is influenced by advection, diffusion, pressure, buoyancy, and Coriolis terms. The pressure terms are written in the familiar form separating the so-called ‘‘pressure-diffusion’’ and ‘‘pressure-strain’’ terms. The viscous terms include transport and dissipation terms. Several advection terms appear due to the rearrangement of the equations, one of which is the triple velocity correlation term. It is desirable that a model for the SFS stresses capture the effect of all of these terms. Note that these equations involve the full velocity and pressure fields, as no decomposition has been made. If the Reynolds decomposition is performed, separating all terms into average and fluctuating components, and the averaging rules of the Reynolds-Averaged Navier-Stokes equations are used, equation (4) reduces to the well-known Reynolds stress evolution equation. There the ‘‘pressure strain’’ and other familiar terms arise as correlations of fluctuating variables instead of the full variables.

Equation (4) is not closed because new correlation terms have appeared; if we are to obtain an expression for τ_{ik} to be used in the resolved flow equation (2), we must make approximations to relate the unclosed terms to known terms from the resolved flow. The traditional procedure has been to use scaling and physical arguments to model the unclosed terms. Here, we follow a purely mathematical approach to obtain an approximate solution to these equations. With that aim, we introduce a multi-dimensional Taylor expansion for the velocity, density, and pressure fields at any point, *e.g.*,

$$u_i(x'_j) \approx u_i(x_j) + (x'_m - x_m) \frac{\partial u_i(x_j)}{\partial x_m} + \frac{1}{2} (x'_m - x_m)(x'_n - x_n) \frac{\partial^2 u_i(x_j)}{\partial x_m \partial x_n} + \dots , \tag{5}$$

using index notation for compactness. The Taylor expansion was used in this way over twenty years ago by Leonard [3].

We now apply an anisotropic Gaussian filter:

$$\overline{u_i}(x, y, z) = \int_{-\infty}^{\infty} \int_{-\infty}^{\infty} \int_{-\infty}^{\infty} G(x - x', y - y', z - z') u_i(x', y', z') dx' dy' dz' \tag{6}$$

where

$$G(x, y, z) = \frac{6^{3/2}}{\pi^{3/2} \Delta_x^2 \Delta_y^2 \Delta_z^2} \exp\left(-\frac{6x^2}{\Delta_x^2} - \frac{6y^2}{\Delta_y^2} - \frac{6z^2}{\Delta_z^2}\right) \quad (7)$$

and $\Delta_x, \Delta_y, \Delta_z$ are the filter sizes in each direction. Other filters could be used here, including asymmetric filters, with a change in the expansion coefficients below. (However, see the consequences of the use of the spectral cutoff filter discussed in the following sections.) The Gaussian filter eliminates all terms with odd powers of $x, y,$ or $z,$ due to symmetry, so that

$$\begin{aligned} \bar{u}_i(x, y, z) &= u_i + \frac{\Delta_x^2}{24} \frac{\partial^2 u_i}{\partial x^2} + \frac{\Delta_y^2}{24} \frac{\partial^2 u_i}{\partial y^2} + \frac{\Delta_z^2}{24} \frac{\partial^2 u_i}{\partial z^2} + \frac{\Delta_x^4}{1152} \frac{\partial^4 u_i}{\partial x^4} + \frac{\Delta_y^4}{1152} \frac{\partial^4 u_i}{\partial y^4} + \frac{\Delta_z^4}{1152} \frac{\partial^4 u_i}{\partial z^4} \\ &+ \frac{\Delta_x^2 \Delta_y^2}{1728} \frac{\partial^4 u_i}{\partial x^2 \partial y^2} + \frac{\Delta_y^2 \Delta_z^2}{1728} \frac{\partial^4 u_i}{\partial y^2 \partial z^2} + \frac{\Delta_x^2 \Delta_z^2}{1728} \frac{\partial^4 u_i}{\partial x^2 \partial z^2} + O(\Delta^6). \end{aligned} \quad (8)$$

Asymmetric filters would give a more complex expression because all derivative terms would be retained. Rearranging and using this expression recursively, we obtain

$$\begin{aligned} u_i(x, y, z) &\approx \bar{u}_i(x, y, z) - \frac{\Delta_x^2}{24} \frac{\partial^2 \bar{u}_i}{\partial x^2} - \frac{\Delta_y^2}{24} \frac{\partial^2 \bar{u}_i}{\partial y^2} - \frac{\Delta_z^2}{24} \frac{\partial^2 \bar{u}_i}{\partial z^2} + \frac{\Delta_x^4}{1152} \frac{\partial^4 \bar{u}_i}{\partial x^4} + \frac{\Delta_y^4}{1152} \frac{\partial^4 \bar{u}_i}{\partial y^4} + \frac{\Delta_z^4}{1152} \frac{\partial^4 \bar{u}_i}{\partial z^4} \\ &+ \frac{5\Delta_x^2 \Delta_y^2}{1728} \frac{\partial^4 \bar{u}_i}{\partial x^2 \partial y^2} + \frac{5\Delta_y^2 \Delta_z^2}{1728} \frac{\partial^4 \bar{u}_i}{\partial y^2 \partial z^2} + \frac{5\Delta_x^2 \Delta_z^2}{1728} \frac{\partial^4 \bar{u}_i}{\partial x^2 \partial z^2} + O(\Delta^6), \end{aligned} \quad (9)$$

which expresses the full velocity at a point (x, y, z) in terms of the filtered velocity at that point. If the filter is isotropic, (9) reduces to

$$\begin{aligned} u_i(x, y, z) &\approx \bar{u}_i(x, y, z) - \frac{\Delta^2}{24} \nabla^2 \bar{u}_i + \frac{\Delta^4}{1152} \left(\frac{\partial^4 \bar{u}_i}{\partial x^4} + \frac{\partial^4 \bar{u}_i}{\partial y^4} + \frac{\partial^4 \bar{u}_i}{\partial z^4} \right) \\ &+ \frac{5\Delta^4}{1728} \left(\frac{\partial^4 \bar{u}_i}{\partial x^2 \partial y^2} + \frac{\partial^4 \bar{u}_i}{\partial y^2 \partial z^2} + \frac{\partial^4 \bar{u}_i}{\partial x^2 \partial z^2} \right) + O(\Delta^6). \end{aligned} \quad (10)$$

This simplified form of the Taylor expansion will be used in the remaining derivations, as the anisotropic form is more cumbersome algebraically. Terms of $O(\Delta^4)$ and higher will also be ignored subsequently. The anisotropic results to fourth order can be recovered by replacing $\frac{\Delta^2}{24} \nabla^2$ by

$$\frac{\Delta_x^2}{24} \frac{\partial^2}{\partial x^2} + \frac{\Delta_y^2}{24} \frac{\partial^2}{\partial y^2} + \frac{\Delta_z^2}{24} \frac{\partial^2}{\partial z^2}. \quad (11)$$

Generation of expanded evolution equations for τ_{ij}

In Reynolds-averaged modeling, the evolution equations for τ_{ij} are often simplified by neglecting various terms. It is therefore of interest to determine the importance of these terms in the evolution of the SFS stress as given by (4). To obtain a closed form of the equations, we now substitute the expansion in equation (10) (and similar expansions for pressure and density) into the unclosed terms in equation (4) and simplify. The evolution equation for τ_{ik} , accurate to $O(\Delta^4)$, is then

$$\frac{\partial \tau_{ik}}{\partial t} + \bar{u}_j \frac{\partial \tau_{ik}}{\partial x_j} = -\bar{u}_j \frac{\partial \overline{u_i u_k}}{\partial x_j} + \frac{\Delta^2}{24} \left(\bar{u}_j \frac{\partial \overline{u_i \nabla^2 u_k}}{\partial x_j} \right) + \frac{\Delta^2}{24} \left(\bar{u}_j \frac{\partial \overline{u_k \nabla^2 u_i}}{\partial x_j} \right) + \frac{\Delta^2}{24} \left(\nabla^2 \bar{u}_j \frac{\partial \overline{u_i u_k}}{\partial x_j} \right)$$

$$\begin{aligned}
& + \overline{u}_j \frac{\partial \overline{u_i u_k}}{\partial x_j} - \frac{\Delta^2}{24} \overline{u}_j \left(\frac{\partial \overline{u_i \nabla^2 u_k}}{\partial x_j} \right) - \frac{\Delta^2}{24} \overline{u}_j \left(\frac{\partial \overline{u_k \nabla^2 u_i}}{\partial x_j} \right) + \overline{u}_k \frac{\partial \tau_{ij}}{\partial x_j} + \overline{u}_i \frac{\partial \tau_{kj}}{\partial x_j} \\
& - \frac{1}{\rho_0} \left[\frac{\partial \overline{u_k \overline{P}}}{\partial x_i} - \frac{\Delta^2}{24} \left(\frac{\partial \overline{P \nabla^2 u_k}}{\partial x_i} \right) - \frac{\Delta^2}{24} \left(\frac{\partial \overline{u_k \nabla^2 \overline{P}}}{\partial x_i} \right) - \frac{\partial \overline{u_k \overline{P}}}{\partial x_i} \right. \\
& + \left. \frac{\partial \overline{u_i \overline{P}}}{\partial x_k} - \frac{\Delta^2}{24} \left(\frac{\partial \overline{P \nabla^2 u_i}}{\partial x_k} \right) - \frac{\Delta^2}{24} \left(\frac{\partial \overline{u_i \nabla^2 \overline{P}}}{\partial x_k} \right) - \frac{\partial \overline{u_i \overline{P}}}{\partial x_k} \right] \\
& + \frac{1}{\rho_0} \left[\overline{P} \frac{\partial \overline{u_k}}{\partial x_i} - \frac{\Delta^2}{24} \left(\overline{P} \frac{\partial \nabla^2 \overline{u_k}}{\partial x_i} \right) - \frac{\Delta^2}{24} \left((\nabla^2 \overline{P}) \frac{\partial \overline{u_k}}{\partial x_i} \right) - \overline{P} \frac{\partial \overline{u_k}}{\partial x_i} \right. \\
& + \left. \overline{P} \frac{\partial \overline{u_i}}{\partial x_k} - \frac{\Delta^2}{24} \left(\overline{P} \frac{\partial \nabla^2 \overline{u_i}}{\partial x_k} \right) - \frac{\Delta^2}{24} \left((\nabla^2 \overline{P}) \frac{\partial \overline{u_i}}{\partial x_k} \right) - \overline{P} \frac{\partial \overline{u_i}}{\partial x_k} \right] \\
& + \nu \frac{\partial^2 \tau_{ik}}{\partial x_j \partial x_j} - 2\nu \frac{\partial \overline{u_i}}{\partial x_j} \frac{\partial \overline{u_k}}{\partial x_j} + \nu \frac{\Delta^2}{12} \frac{\partial \overline{u_i}}{\partial x_j} \frac{\partial \nabla^2 \overline{u_k}}{\partial x_j} + \nu \frac{\Delta^2}{12} \frac{\partial \nabla^2 \overline{u_i}}{\partial x_j} \frac{\partial \overline{u_k}}{\partial x_j} + 2\nu \frac{\partial \overline{u_i}}{\partial x_j} \frac{\partial \overline{u_k}}{\partial x_j} \\
& - \frac{g}{\rho_0} \left(\frac{\overline{\rho u_k}}{\rho_0} - \frac{\Delta^2}{24} \frac{\overline{\rho \nabla^2 u_k}}{\rho_0} - \frac{\Delta^2}{24} \frac{\overline{u_k \nabla^2 \rho}}{\rho_0} - \overline{\rho u_k} \right) \delta_{i3} \\
& - \frac{g}{\rho_0} \left(\frac{\overline{\rho u_i}}{\rho_0} - \frac{\Delta^2}{24} \frac{\overline{\rho \nabla^2 u_i}}{\rho_0} - \frac{\Delta^2}{24} \frac{\overline{u_i \nabla^2 \rho}}{\rho_0} - \overline{\rho u_i} \right) \delta_{k3} \\
& + f_n (\epsilon_{imn} \tau_{mk} + \epsilon_{kmn} \tau_{mi}) . \tag{12}
\end{aligned}$$

Eqs. (12) are a closed set of equations for τ_{ik} ; the contribution of all the filtered quantities to the evolution of τ_{ik} can be explicitly computed. Such a set of equations could be solved for the six independent components of τ_{ik} , without need for further simplifications or assumptions. Although feasible, this would add a significant computational expense to the solution of the resolved flow equation (2). The solution obtained for \overline{u}_i would be accurate to $O(\Delta^4)$.

Generation of the τ_{ij} models

In the spirit of velocity estimation models, instead of solving six more equations for τ_{ik} , we derive models for τ_{ij} by substituting the series expansion for the velocity (10) directly into (3). When the unclosed term is expanded, and terms fourth order and higher are neglected, we obtain

$$\text{Model 1: } \tau_{ik} = \overline{u_i u_k} - \overline{u_i} \overline{u_k} - \frac{\Delta^2}{24} \overline{u_i \nabla^2 u_k} - \frac{\Delta^2}{24} \overline{u_k \nabla^2 u_i} . \tag{13}$$

If the explicit term, $\overline{u_i u_j}$, is also expanded, the representation becomes

$$\text{Model 2: } \tau_{ik} = \overline{u_i u_k} - \overline{u_i} \overline{u_k} - \frac{\Delta^2}{24} \overline{u_i \nabla^2 u_k} - \frac{\Delta^2}{24} \overline{u_k \nabla^2 u_i} + \frac{\Delta^2}{24} \overline{u_i \nabla^2 u_k} + \frac{\Delta^2}{24} \overline{u_k \nabla^2 u_i} . \tag{14}$$

To second order in the filter width, equation (14) reduces to the Bardina scale-similarity model. This scale-similarity property of (14) will later be shown to have desirable effects (see *a priori* test section). The higher order terms that are not present in the Bardina model can be shown to be dissipative [21]. Further properties of these two models will be discussed in the sections that follow.

Though we did not directly solve the evolution equations for τ_{ik} , we can substitute equation (13) into the evolution equation (12) to demonstrate that it is indeed a solution, as the resulting equation is the sum of the evolution equations for the components of (13). It is perhaps more straightforward to construct the evolution equation for the approximate form (13) and show that it is the same as (12). This is done by a similar procedure used to derive equation (4). After adding and subtracting the evolution equations for each of the terms that make up the approximate τ_{ik} , and simplifying using the series expansion introduced previously to effectively “unbar” certain terms (see text leading to equation (31) in the Appendix), we obtain (12) to $O(\Delta^4)$. Thus, to fourth-order accuracy in the filter width, Δ , we have a solution for the subfilter-scale stresses, τ_{ik} . As can be shown by a similar procedure, equation (14) is a solution, to fourth order, of the analogous version of (12) obtained when the closed terms are expanded as well. Note that the evolution equation developed for the approximate τ_{ik} indicates that these subfilter-scale stresses are influenced by buoyancy and Coriolis forces, as well as diffusion, pressure and advection terms, just as the resolved velocities are. Thus the expressions (13) and (14) for τ_{ik} capture the effects of all of the relevant physical mechanisms, to fourth order in the filter width.

Two final observations are worthwhile. First, the preceding analysis can be carried out with any spatially homogeneous filter. Indeed, up to fourth order in the filter width, the analytical results for the tophat filter (see equations (16) and (17) below) are identical. However, special consideration is needed if a spectral cutoff filter is used. As concluded by Domaradzki and Saiki [11] after examining several analyses and theories, “the SGS energy transfer is dominated by energy exchanges among resolved and unresolved scales from the vicinity of the cutoff.” Thus, as Leonard [3] pointed out, “large wave-number Fourier modes need the assistance of small wave-number modes to transfer energy from large scales to small scales. In the Fourier method the sharp cutoff in wave-number space precludes such a transfer.” Accordingly, the sharp-cutoff filter is ill-suited to velocity estimation methods, including the series expansion model presented here. If it were used, two different cutoff wavenumbers would be needed for terms filtered more than once to prevent the Bardina term from disappearing [5].

Second, any fourth-order approximation to the full velocity in terms of the resolved field would yield a SFS stress model accurate to fourth order in the filter width. The nice feature of the series expansion model used above is that if the velocity field is sufficiently smooth, the fourth-order approximation is a simple mathematical expression that does not involve empirical modeling.

Rudimentary tests of the model

Following the example of Geurts [13], we perform a modified wave number analysis of the models (13) and (14). We consider one mode of a velocity field, $u = \exp(ikx)$, and evaluate the one-dimensional SFS stress,

$$\tau = \overline{u^2} - \bar{u}^2 . \quad (15)$$

We use two different filters, defined in one-dimensional form as

$$\bar{f}(x) = \int_{-\infty}^{\infty} H(x-x')f(x')dx' \quad (16)$$

where

$$H_G(x) = \sqrt{\frac{6}{\pi\Delta^2}} \exp\left(-\frac{6x^2}{\Delta^2}\right) \quad ; \quad H_T(x) = \begin{cases} 1/\Delta & \text{for } |x| \leq \Delta/2 \\ 0 & \text{for } |x| > \Delta/2 \end{cases} \quad (17)$$

for the Gaussian filter and the tophat filter, respectively. The filtered velocity takes the form

$$\bar{u} = G(k\Delta) \exp(ikx) , \quad (18)$$

where

$$G_G(k\Delta) = \exp\left(-\frac{k^2\Delta^2}{24}\right) \quad ; \quad G_T(k\Delta) = \frac{\sin k\Delta/2}{k\Delta/2} , \quad (19)$$

for the Gaussian and tophat filters, respectively. The series expansion used to represent the unfiltered velocity becomes

$$u^* = A(k\Delta)G(k\Delta) \exp(ikx) , \quad (20)$$

where

$$A_G(k\Delta) = \left(1 + \frac{k^2\Delta^2}{24} + \frac{k^4\Delta^4}{1152}\right) \quad (21)$$

for the Gaussian filter, and

$$A_T(k\Delta) = \left(1 + \frac{k^2\Delta^2}{24} + \frac{7k^4\Delta^4}{5760}\right) \quad (22)$$

for the tophat filter. The truncation order of $A(k\Delta)$ can be specified, and is $O(\Delta^6)$ above.

In Figure 1 we plot the amplitude, $A(k\Delta)G(k\Delta)$, of (20) versus $k\Delta$ for the two filters with different truncation orders of the expansion in $A(k\Delta)$. This corresponds to figure 1 in [13]. The fourth-order accurate approximation (6th-order truncation error) gives the best results. In all cases, the amplitude deviation from 1 increases with $k\Delta$, but the agreement is good for $k\Delta < \pi$, the range of interest. In particular, the Gaussian filter gives a much better approximation to the full velocity than the tophat filter, especially at higher k , as the filter is smooth in both physical and Fourier space, and includes the influence of a broader range of the velocity field. The tophat filter oscillates in Fourier space and hence introduces spurious higher modes into the filtered velocity field.

The exact form of the SFS stress for $u = \exp(ikx)$ is

$$\tau_G = [G_G(2k\Delta) - G_G^2(k\Delta)] \exp(2ikx) , \quad (23)$$

for the Gaussian filter, and

$$\tau_T = \frac{1}{2} [1 - G_T^2(k\Delta)] - \frac{1}{2} [G_T(2k\Delta) - G_T^2(k\Delta)] \exp(2ikx) , \quad (24)$$

for the tophat filter, which is the equation given by Geurts [13]. The approximate forms are found by using the estimate of the unfiltered velocity given in (20) to obtain the 1-D representation of (13):

$$\text{Model 1: } \tau_{M1} = \overline{u^{*2}} - \bar{u}^2 , \quad (25)$$

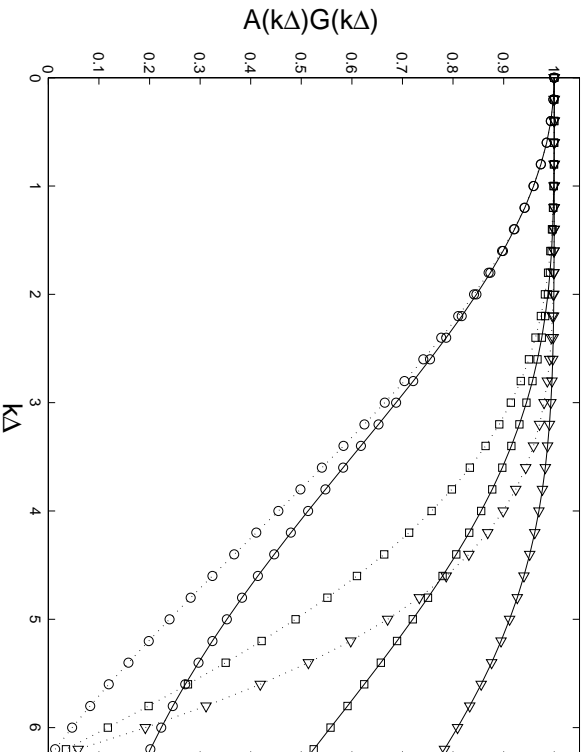


Figure 1: Amplitude of velocity estimates. Solid line: Gaussian filter, dotted line: tophat filter. \circ : 2nd order; \square : 4th order; \triangleright : 6th order.

so that

$$\tau_{GM1} = G_G^2(k\Delta) [A_G^2(k\Delta)G_G(2k\Delta) - 1] \exp(2ikx), \quad (26)$$

$$\tau_{TM1} = \frac{1}{2}G_T^2(k\Delta) [A_T^2(k\Delta) - 1 - (A_T^2(k\Delta)G_T(2k\Delta) - 1) \exp(2ikx)]. \quad (27)$$

Alternatively, if we also use the approximate velocity (20) in the calculation of the second term in (15), as done in (14), we obtain

$$\text{Model 2: } \tau_{M2} = \overline{u^{*2}} - \overline{u^{*2}}, \quad (28)$$

and

$$\tau_{M2} = A^2(k\Delta)G^2(k\Delta) \tau, \quad (29)$$

for both the tophat and Gaussian filters. This approximate form is simply the application of the filter and expansion operators, $A(k\Delta)G(k\Delta)$, on τ twice.

The amplitude of the oscillating parts of τ_{GM1} , τ_{TM1} , and τ_{M2} are shown in figures 2-5 for different truncation orders of the models. The approximate forms are shown versus the amplitudes of the oscillating parts of the exact τ given in equations (23) and (24) for each filter. Again, the agreement for $k\Delta < \pi$ is good. Of the models for τ , Model 1 seems to perform better than Model 2, and the Gaussian filter models are more effective than the tophat models in representing the subfilter stress at higher wave numbers. Figures 6 and 7 show a comparison of Model 1 and Model 2 for each filter type. It is seen that for the Gaussian filter, Model 1 is very close to the exact subfilter stress, and Model 2 is also quite good. Model 1 also performs better than Model 2 for the tophat filter.

The tophat filter version in (29) shown in figure 3 can be compared to figure 2 in Geurts [13]. The fourth-order model derived here gives results comparable to or perhaps slightly

better than the case $L = 2$ in [13]. As was done by Geurts, this test could be extended to the general case $u = \sum_k \exp(ikx)$ to provide similar information about the velocity approximation, but we shall not do this.

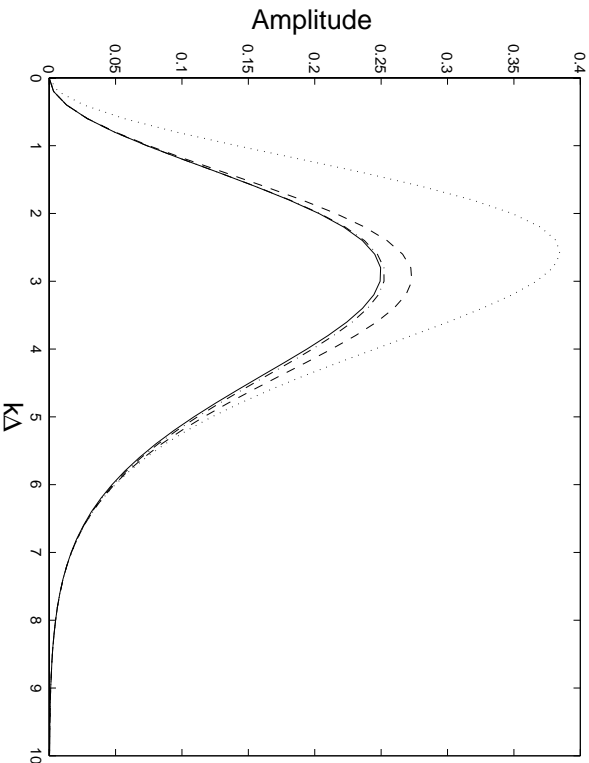


Figure 2: Amplitude of τ_{GM1} (Gaussian filter) and exact τ . Solid line: exact; dotted line: 2nd-order model; dashed line: 4th-order model; dash-dotted line: 6th-order model.

A priori tests

A more robust preliminary test of the subfilter-scale model is provided by an *a priori* test [22, 1, 15], in which data from a direct numerical simulation (DNS) are filtered and compared to the model. *A priori* tests indicate the degree of correlation between the modeled and exact subfilter-scale terms and are useful indications of the expected performance of a SFS model in actual LES computations (*a posteriori* tests). Comparisons can be made at the tensor (τ_{ij}), vector ($\partial\tau_{ij}/\partial x_j$), and scalar ($\tau_{ij}\partial u_i/\partial x_j$) levels.

Although a high correlation (close to one) with the exact value is not a sufficient condition for a good SFS model, it is certainly a desirable feature. Of the commonly used SFS models, it is known that the Smagorinsky model does poorly in *a priori* tests, as the modeled τ_{ij} is not aligned with the actual stress tensor. The Smagorinsky model is, however, able to provide adequate dissipation and thus performs fairly well in some actual LES. Scale-similarity models (*e.g.* the Bardina model), on the other hand, display very good correlations, but do not dissipate enough energy when implemented in LES. *A posteriori* tests are necessary to obtain complete information on a model’s performance and, in particular, on the actual level of energy dissipation. An *a posteriori* test, using this SFS model in an LES simulation, is currently being undertaken by L. Ding in our laboratory. However, ratios between modeled and exact quantities (particularly at the scalar level) obtained from *a priori* tests provide a quick assessment as to whether the model provides adequate dissipation.

The DNS dataset used here is from the sheared and stably-stratified homogeneous turbulent flow computations performed by Shih *et al.* [23]. The Reynolds number based on the

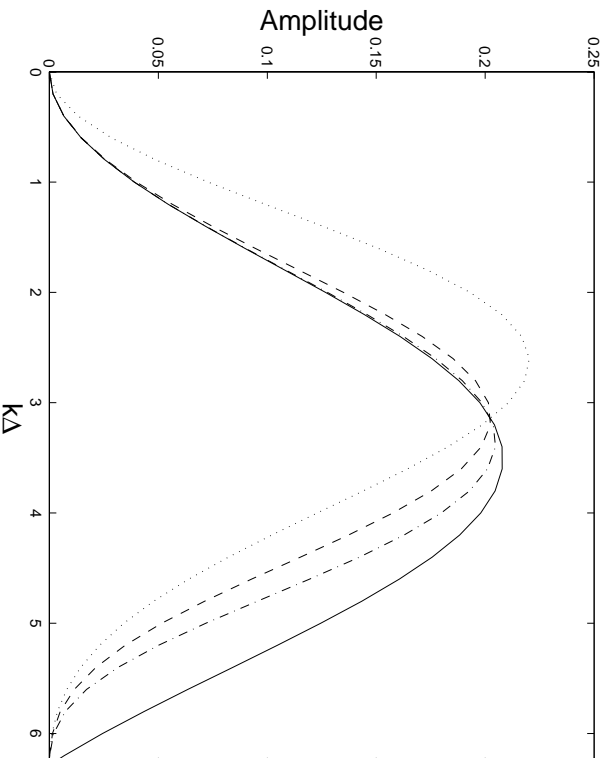


Figure 3: Amplitude of $\tau_{T_{M1}}$ (tophat filter) and exact τ . Solid line: exact; dotted line: 2nd-order model; dashed line: 4th-order model; dash-dotted line: 6th-order model.

Taylor microscale is 89.44, the Richardson number is 0.16, and the nondimensional shear number is 2.0. The DNS data, u_i , are defined on a 128^3 grid with domain size $2\pi^3$ where $\Delta_{DNS} < \Delta_{LES}$. The DNS grid is anisotropic due to coordinate stretching factors used for computation of the homogeneous shear flow. Here, x_1 is the streamwise direction, x_2 is the vertical direction, and x_3 is the spanwise shear flow. Here, shear is applied in the x_1, x_2 -plane. The DNS data are sampled on the scale of the LES grid and filtered using a Gaussian filter of width $\Delta = 2\Delta_{LES}$ to obtain the LES field, \bar{u}_i . This filter-grid ratio is chosen so that the discretization errors in an actual LES would be smaller than the contribution of the SFS terms [2]. Since the DNS data represent the exact velocity field, the exact subfilter-scale stress can be computed at each point on the grid. The modeled SFS stress can be computed from the LES field defined on the LES grid, and compared to the exact stress at the same points on the LES grid. The correlation coefficient and the ratio of the rms values are then computed for each of the SFS stress components. The correlation coefficient measures the degree of linearity in the relationship between the modeled and exact SFS stress, while the ratio gives information about the coefficient of proportionality.

Tables 1-3 show correlation coefficients (C) and ratios (R) for selected subfilter-scale quantities: τ_{12} is the SFS shear stress in the shear flow, $\partial\tau_{1j}/\partial x_j$ is the divergence of the subfilter stress which appears in the momentum equations, and $\tau_{ij}\partial u_i/\partial x_j$ is the SFS stress dissipation. The ratio is the exact DNS rms value divided by the modeled rms value, and should be close to one. For the dissipation term, the ratio gives an indication of the magnitude of energy dissipated by the model. Results are presented for the following subfilter-scale models: Smagorinsky (S), Bardina scale-similarity (B), modified Clark (MC), 4th-order series expansion using (13) (T4), modified 4th-order series expansion using (14) (MT4), and modified 6th-order series expansion using (14) (MT6). The models are given in the Appendix. LES to DNS grid ratios of $GR = 2, 4, 8$ are considered, where $\Delta_{LES} = GR \Delta_{DNS}$. In each case the filter-grid ratio is $FGR = \Delta/\Delta_{LES} = 2$.

The correlations for the Bardina scale-similarity model are quite high; however, the ratios

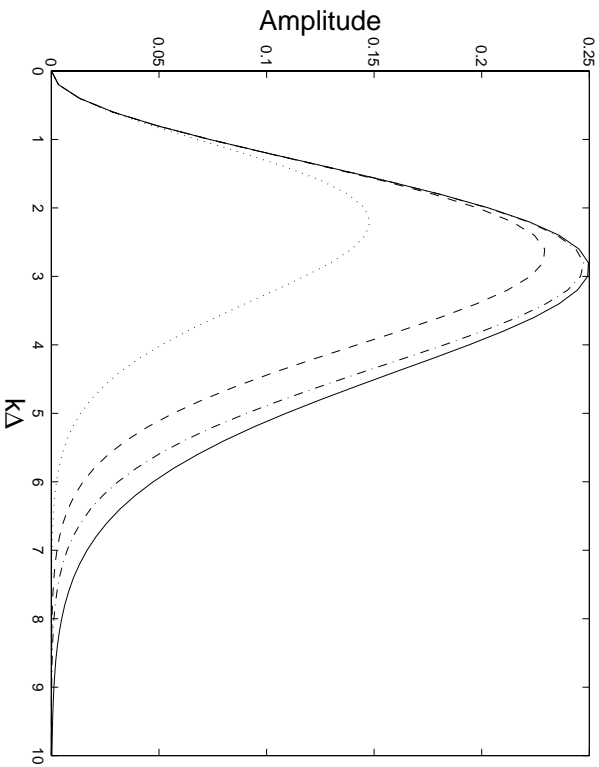


Figure 4: Amplitude of τ_{GM2} (Gaussian filter) and exact τ . Solid line: exact; dotted line: 2nd-order model; dashed line: 4th-order model; dash-dotted line: 6th-order model.

are not very good, indicating that the model does not capture energy dissipation correctly, as noted previously. The Smagorinsky model does not perform well at all; however, the ratio for the dissipation is better than that for the Bardina model for $GR = 4, 8$. The MT4 model contains the scale-similarity terms of the Bardina model, while model T4 does not. It seems that the inclusion of these terms significantly improves the correlation coefficients; however, the improvement in the ratios is more evident only in the 6th-order representation, MT6. (This is also seen in the single mode tests done in the previous section: Model 1 performs better than Model 2, which has the Bardina model form, in amplitude comparisons.) The modified Clark model, derived from the T4 model, performs comparably to the other series expansion models, often with slightly higher correlations but poorer ratios.

The correlations are highest for the MT6 model, the 6th-order expression for the series expansion model, with values over 0.99 for $GR = 2$. Ratios as good as 1.0062 are obtained for the SFS dissipation modeled with MT6 showing that the dissipation is captured to within 1% of the exact value. The correlation decreases when the LES grid becomes coarser, *i.e.*, as GR increases and the resolved scale wavenumber cutoff becomes smaller; it is harder to represent the higher wavenumbers with a smaller range of resolved scales. This is an important limitation, because we would like to apply LES to large domains and Reynolds numbers for which the LES to DNS grid ratio is necessarily high. However, even at $GR = 8$, the MT6 model captures most of the SFS stress, and has a correlation of 0.9422, significantly higher than the other models. Though the discretization error of the numerical scheme used in many actual LES is larger than 6th order, it may help to use a more accurate SFS model such as MT6. Similar results to those in tables 1-3 are obtained when a tophat filter is used, though the numbers are not quite as good overall.

The results from this *a priori* analysis compare very favorably with *a priori* tests performed by others for their models, *e.g.*, Domaradzki and Saiki [11], Stolz and Adams [24], and Salvetti *et al.* [25]. For a compressible ramp flow (with $GR = 2$ and $FGR = 2$), Stolz and Adams [24] obtained correlations of approximately 0.99 (as we do) for their approximate deconvolution model using seven terms in an inverse filter expansion.

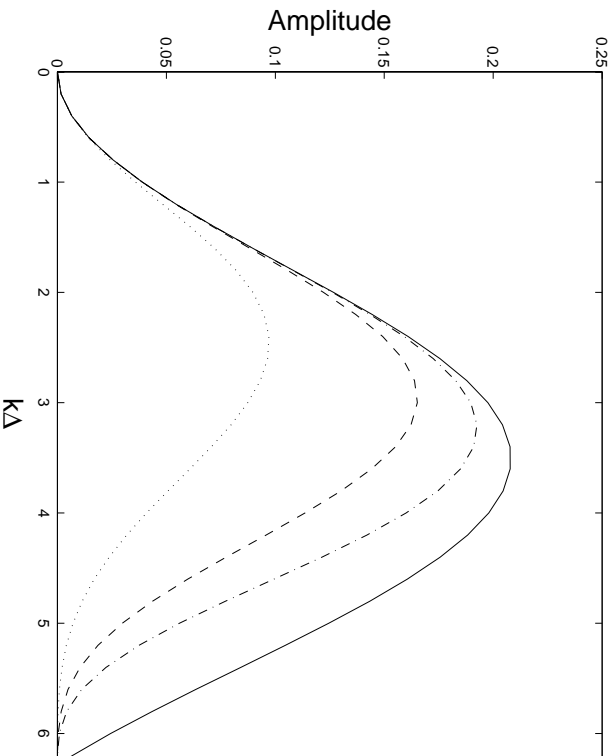


Figure 5: Amplitude of τ_{TM2} (tophat filter) and exact τ . Solid line: exact; dotted line: 2nd-order model; dashed line: 4th-order model; dash-dotted line: 6th-order model.

As an illustration of the ability of this velocity estimation model (9) to represent the full velocity field, figure 8 shows contours of the streamwise velocity for different truncation orders in the velocity estimation. The raw DNS data, which is sampled on the LES grid defined by the parameter GR , is best represented by the highest order model, MT6; unlike the lower order models, velocity contours for this case capture the smaller features of the DNS data quite well.

Implementation of model

One of the most attractive features of the series expansion model is its ease of implementation. The form of the SFS stress model is given by equation (13) or (14), which can be directly computed and substituted into the resolved flow equation. Equation (2) must then be discretized and solved numerically, *e.g.* by the method of Zang *et al.* [26]. The computational cost of using this SFS model will be comparable to the cost of the S^3 model [10]. Preliminary results for the series model indicate that its CPU requirement is significantly less than or about equal to that for the dynamic two-parameter model [27, 19], depending (it appears) on whether the grid is a Cartesian grid or a mapped grid where the metrics add to the cost of computing the model terms. The greatest difficulty will be implementation of the model near solid boundaries, where care must be taken in representing higher order terms for the 6th-order model. This issue is currently under investigation.

Because the SFS stress tensor is $O(\Delta^2)$ (see Appendix), it is important that the filter width, Δ , be larger than the grid size upon which discretization is performed. Otherwise, numerical discretization error in a second-order scheme will have an effect of the same order of magnitude as the SFS stress. The analysis of Ghosal [2] indicates that choosing the filter width to be at least twice the grid size is advisable.

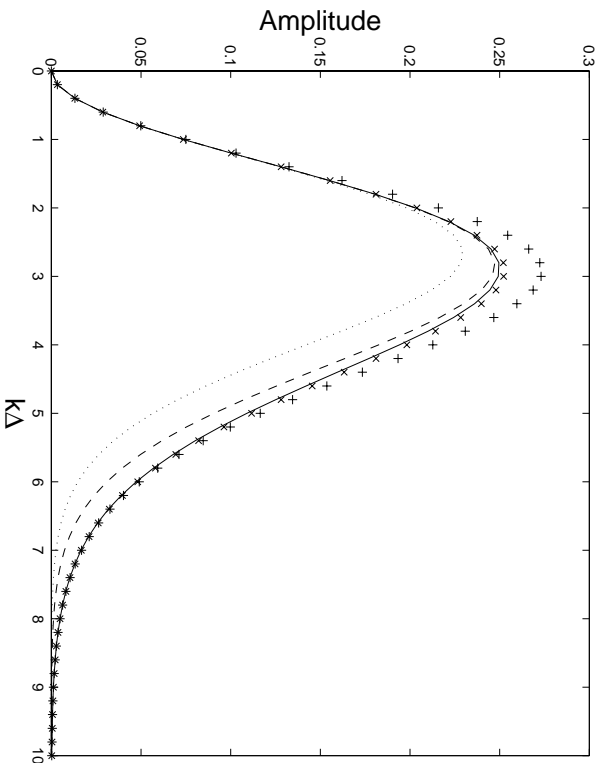


Figure 6: Amplitude of τ_{GM1} , τ_{GM2} (Gaussian filter) and exact τ . Solid line: exact; ++++: 4th-order Model 1; $\times \times \times$: 6th-order Model 1; dotted line: 4th-order Model 2; dashed line: 6th-order Model 2.

As noted above, the tophat filter can also be used with the series expansion in three-dimensions, as was done in one dimension above. Up to fourth order, the Gaussian and tophat filters give the same expansions, which leads to identical SFS model expressions, but different numerical results because of the different behaviors of the filters. The *a priori* tests show that the Gaussian filter, whose effective width is the same as that of the tophat filter, yields superior results. However, there is not much difference in the numerical approximation of these filters, as the Gaussian filter must be truncated, and it may be hard to distinguish between the discrete representations of these filters when implemented in a finite difference or finite volume simulation. In principle, any filter could be used, as long as it allows interaction of the smallest resolved and largest unresolved scales as discussed previously (requiring, therefore, two different filter cutoffs if the spectral cutoff filter is used). This means that the approach described here for subfilter-scale modeling could accommodate a commuting filter, allowing implementation of this model on non-uniform grids.

Conclusion

As LES begins to be applied to problems in which more of the energy of the flow is unresolved, the accuracy of the SFS model becomes increasingly important. The series expansion model proposed here does not assume that the SFS motions are isotropic, and the model can easily be implemented with an anisotropic filter. Indeed, *a priori* test results for an anisotropic case show very high correlations and ratios between the modeled SFS stress and the exact stress computed from DNS data, indicating that the model captures SFS motions quite accurately. Furthermore, the model satisfies the evolution equation for the SFS stress to an arbitrarily-chosen order in the filter width (4th and 6th orders are used here), making it clear that this SFS model can account for the effects of buoyancy, Coriolis, and pressure forces. There are of course small scale phenomena present in combustion or shocks that present

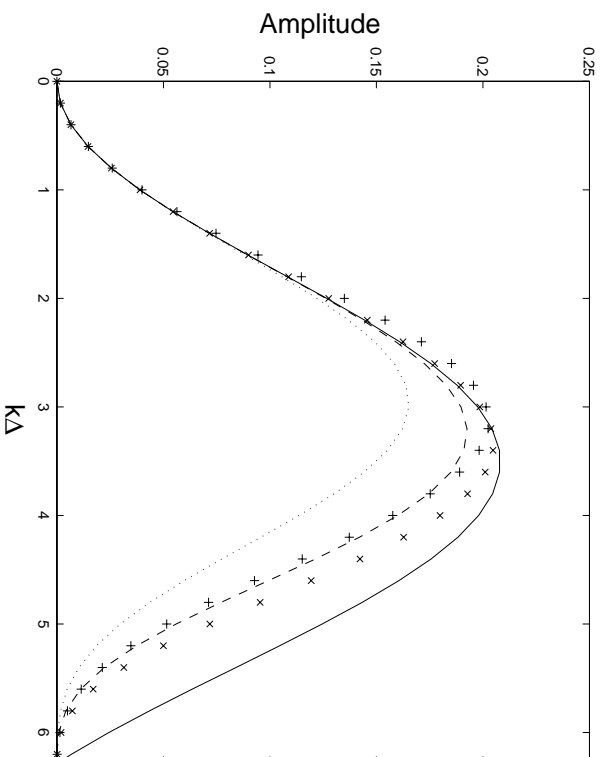


Figure 7: Amplitude of T_{TM1} , T_{TM2} (Gaussian filter) and exact τ . Solid line: exact; +++: 4th-order Model 1; $\times \times \times$: 6th-order Model 1; dotted line: 4th-order Model 2; dashed line: 6th-order Model 2.

further challenges for SFS modeling, as this series model will likely have difficulty with the non-smooth velocity fields of those cases. However, this SFS model is attractive because it does not introduce any parameters, being based on a mathematical expansion. The model can be implemented numerically with ease, and can also be extended to higher accuracy as desired.

Acknowledgments

The support of a National Defense Science and Engineering Graduate fellowship [FVK] and NSF Grant ATM-952646 (Physical Meteorology Program: R.R. Rogers, Program Director) [RLS] is gratefully acknowledged.

		τ_{12}	$\frac{\partial \tau_{1j}}{\partial x_j}$	$\tau_{ij} \frac{\partial u_i}{\partial x_j}$
S	C	0.1610	0.4746	0.6962
	R	3.5042	2.8092	1.4780
B	C	0.9525	0.9194	0.9665
	R	1.3367	1.9179	1.3666
MC	C	0.9602	0.7981	0.9700
	R	1.2927	1.9024	1.3158
T4	C	0.9239	0.9135	0.9430
	R	1.0352	1.1037	1.0790
MT4	C	0.9875	0.9763	0.9917
	R	1.0702	1.2636	1.0724
MT6	C	0.9969	0.9937	0.9972
	R	1.0097	1.0611	1.0062

Table 1: Gaussian Filter: Correlations, GR = 2, FGR = 2.

Appendix

The forms of the models considered in the *a priori* tests are given below:

S: Smagorinsky

$$\tau_{ij} = -2(C_S \Delta)^2 (\overline{S_{ij}} \overline{S_{ij}})^{1/2} \overline{S_{ij}}$$

B: Bardina scale-similarity

$$\tau_{ij} = \overline{\overline{u_i} \overline{u_j}} - \overline{\overline{u_i}} \overline{\overline{u_j}}$$

MC: Modified Clark

$$\tau_{ij} = \frac{\Delta^2}{12} \frac{\partial \overline{u_i}}{\partial x_m} \frac{\partial \overline{u_j}}{\partial x_m}$$

T4: Series expansion, 4th order

$$\tau_{ij} = \overline{\overline{u_i} \overline{u_j}} - \overline{\overline{u_i}} \overline{\overline{u_j}} - \frac{\Delta^2}{24} (\overline{\overline{u_i} \nabla^2 \overline{u_j}} + \overline{\overline{u_j} \nabla^2 \overline{u_i}})$$

MT4: Modified series expansion, 4th order

$$\tau_{ij} = \overline{\overline{u_i} \overline{u_j}} - \overline{\overline{u_i}} \overline{\overline{u_j}} - \frac{\Delta^2}{24} (\overline{\overline{u_i} \nabla^2 \overline{u_j}} + \overline{\overline{u_j} \nabla^2 \overline{u_i}}) + \frac{\Delta^2}{24} (\overline{\overline{u_i} \nabla^2 \overline{u_j}} + \overline{\overline{u_j} \nabla^2 \overline{u_i}}) \quad (30)$$

MT6: Modified series expansion, 6th order

$$\begin{aligned} \tau_{ij} &= \overline{\overline{u_i} \overline{u_j}} - \overline{\overline{u_i}} \overline{\overline{u_j}} - \frac{\Delta^2}{24} (\overline{\overline{u_i} \nabla^2 \overline{u_j}} + \overline{\overline{u_j} \nabla^2 \overline{u_i}}) + \frac{\Delta^2}{24} (\overline{\overline{u_i} \nabla^2 \overline{u_j}} + \overline{\overline{u_j} \nabla^2 \overline{u_i}}) \\ &+ \frac{\Delta^4}{1152} \left(\overline{\overline{u_i} \frac{\partial^4 \overline{u_j}}{\partial x^4}} + \overline{\overline{u_i} \frac{\partial^4 \overline{u_j}}{\partial y^4}} + \overline{\overline{u_i} \frac{\partial^4 \overline{u_j}}{\partial z^4}} + \overline{\overline{u_j} \frac{\partial^4 \overline{u_i}}{\partial x^4}} + \overline{\overline{u_j} \frac{\partial^4 \overline{u_i}}{\partial y^4}} + \overline{\overline{u_j} \frac{\partial^4 \overline{u_i}}{\partial z^4}} \right) \\ &- \frac{\Delta^4}{1152} \left(\overline{\overline{u_i} \frac{\partial^4 \overline{u_j}}{\partial x^4}} + \overline{\overline{u_i} \frac{\partial^4 \overline{u_j}}{\partial y^4}} + \overline{\overline{u_i} \frac{\partial^4 \overline{u_j}}{\partial z^4}} + \overline{\overline{u_j} \frac{\partial^4 \overline{u_i}}{\partial x^4}} + \overline{\overline{u_j} \frac{\partial^4 \overline{u_i}}{\partial y^4}} + \overline{\overline{u_j} \frac{\partial^4 \overline{u_i}}{\partial z^4}} \right) \\ &+ \frac{5\Delta^4}{1728} \left(\overline{\overline{u_i} \frac{\partial^4 \overline{u_j}}{\partial x^2 \partial y^2}} + \overline{\overline{u_i} \frac{\partial^4 \overline{u_j}}{\partial y^2 \partial z^2}} + \overline{\overline{u_i} \frac{\partial^4 \overline{u_j}}{\partial x^2 \partial z^2}} + \overline{\overline{u_j} \frac{\partial^4 \overline{u_i}}{\partial x^2 \partial y^2}} + \overline{\overline{u_j} \frac{\partial^4 \overline{u_i}}{\partial y^2 \partial z^2}} + \overline{\overline{u_j} \frac{\partial^4 \overline{u_i}}{\partial x^2 \partial z^2}} \right) \\ &- \frac{5\Delta^4}{1728} \left(\overline{\overline{u_i} \frac{\partial^4 \overline{u_j}}{\partial x^2 \partial y^2}} + \overline{\overline{u_i} \frac{\partial^4 \overline{u_j}}{\partial y^2 \partial z^2}} + \overline{\overline{u_i} \frac{\partial^4 \overline{u_j}}{\partial x^2 \partial z^2}} + \overline{\overline{u_j} \frac{\partial^4 \overline{u_i}}{\partial x^2 \partial y^2}} + \overline{\overline{u_j} \frac{\partial^4 \overline{u_i}}{\partial y^2 \partial z^2}} + \overline{\overline{u_j} \frac{\partial^4 \overline{u_i}}{\partial x^2 \partial z^2}} \right) \\ &+ \frac{\Delta^4}{576} (\overline{\overline{\nabla^2 u_i} \nabla^2 \overline{u_j}} - \nabla^2 \overline{\overline{u_i}} \nabla^2 \overline{\overline{u_j}}) \end{aligned}$$

		τ_{12}	$\frac{\partial \tau_{1j}}{\partial x_j}$	$\tau_{ij} \frac{\partial u_i}{\partial x_j}$
S	C	0.1557	0.4169	0.6029
	R	3.8231	2.9590	1.5601
B	C	0.8881	0.8748	0.9048
	R	1.6934	2.6138	1.8056
MC	C	0.9082	0.7750	0.9151
	R	1.5108	2.4327	1.6210
$T4$	C	0.8282	0.8013	0.8599
	R	1.1623	1.2721	1.2548
$MT4$	C	0.9544	0.9440	0.9591
	R	1.1800	1.5072	1.2307
$MT6$	C	0.9831	0.9764	0.9831
	R	1.0411	1.1662	1.0663

Table 2: Gaussian Filter: Correlations, GR = 4, FGR = 2.

where \overline{S}_{ij} is the filtered velocity strain tensor, and C_S is the Smagorinsky constant, here taken to be 0.09 [1] (which does not affect correlation values, but does affect ratios). The modified Clark model can be obtained from a rearrangement of the 4th-order series expansion model, as derived below, and is a variation of the model considered by Clark *et al.* [22]. Here filtering is applied to the product of the two derivatives, whereas in the original, each term is separately filtered.

The modified Clark model is derived by “unbarring” terms in the τ_{ik} expansion, *i.e.* removing one level of filtering. This is done by using (10); anywhere terms of the form $\overline{u_i} - \frac{\Delta^2}{24} \nabla^2 \overline{u_i}$ appear, they can be replaced with 2nd-order accuracy by the unfiltered variable u_i . This idea was used to simplify terms in the derivation of the evolution equation (12) for the modeled SFS stress. We now apply “unbarring” to the SFS stress model given in (13). First rewriting the second-derivative terms using the product rule, we have

$$\begin{aligned} \tau_{ik} &= \overline{u_i u_k} - \overline{u_i} \overline{u_k} - \frac{\Delta^2}{24} \overline{u_i \nabla^2 u_k} - \frac{\Delta^2}{24} \overline{u_k \nabla^2 u_i} + O(\Delta^4) \\ \tau_{ik} &= \overline{u_i u_k} - \overline{u_i} \overline{u_k} - \frac{\Delta^2}{24} \nabla^2 \overline{u_i u_k} + \frac{\Delta^2}{12} \frac{\partial \overline{u_k}}{\partial x_j} \frac{\partial \overline{u_i}}{\partial x_j} + O(\Delta^4). \end{aligned}$$

Now “unbarring”, the first and third terms on the right-hand side become $\overline{u_i} \overline{u_j}$, which cancels the second term. We then have

$$\tau_{ik} = \frac{\Delta^2}{12} \frac{\partial \overline{u_k}}{\partial x_j} \frac{\partial \overline{u_i}}{\partial x_j} + O(\Delta^4), \quad (31)$$

which shows that the SFS stress is 2nd-order accurate in the filter width. It can be shown that this form also satisfies the evolution equation for τ_{ik} to fourth order.

		τ_{12}	$\frac{\partial \tau_{ij}}{\partial x_j}$	$\tau_{ij} \frac{\partial u_i}{\partial x_j}$
<i>S</i>	<i>C</i>	0.0925	0.3041	0.3920
	<i>R</i>	4.9880	3.1754	2.0092
<i>B</i>	<i>C</i>	0.7759	0.7852	0.8181
	<i>R</i>	2.8324	4.1177	3.1285
<i>MC</i>	<i>C</i>	0.7960	0.7104	0.8263
	<i>R</i>	2.1099	3.3449	2.4171
<i>T4</i>	<i>C</i>	0.6691	0.6032	0.7470
	<i>R</i>	1.6837	1.7023	1.8542
<i>MT4</i>	<i>C</i>	0.8769	0.8729	0.8939
	<i>R</i>	1.5989	2.0326	1.7325
<i>MT6</i>	<i>C</i>	0.9407	0.9326	0.9422
	<i>R</i>	1.2301	1.4111	1.3038

Table 3: Gaussian Filter: Correlations, GR = 8, FGR = 2.

References

- [1] J. Bardina, J.H. Ferziger, and W.C. Reynolds. Improved turbulence models based on large eddy simulation of homogeneous, incompressible, turbulent flows. Technical Report TF-19, Department of Mechanical Engineering, Stanford University, Stanford, California, 1983.
- [2] S. Ghosal. An analysis of numerical errors in large-eddy simulations of turbulence. *Journal of Computational Physics*, 125:187–206, 1996.
- [3] A. Leonard. Energy cascade in large eddy simulations of turbulent fluid flows. *Advances in Geophysics*, 18A:237–248, 1974.
- [4] J. Smagorinsky. General circulation experiments with the primitive equations. *Monthly Weather Review*, 93:99, 1963.
- [5] Y. Zang, R. L. Street, and J. R. Koseff. A dynamic mixed subgrid-scale model and its application to turbulent recirculating flows. *Physics of Fluids*, 5(12):3186–3196, 1993.
- [6] M. Germano, Piomelli U., Moin P., and Cabot W.H. A dynamic subgrid-scale eddy viscosity model. *Physics of Fluids*, 3(7):1760–1765, 1991.
- [7] U. Piomelli. Large-eddy simulation: achievements and challenges. *Progress in Aerospace Science*, 35(4):335–362, 1999.
- [8] F. Sarghini, U. Piomelli, and E. Balaras. Scale-similar models for large-eddy simulations. *Physics of Fluids*, 11(6):1596–1607, 1999.
- [9] M. Lesieur and O. Métais. New trends in large-eddy simulations of turbulence. *Annual Review of Fluid Mechanics*, 28:45–82, 1996.
- [10] K.B. Shah and J.H. Ferziger. A new non-eddy viscosity subgrid-scale model and its application to channel flow. Annual research briefs, Center for Turbulence Research, NASA Ames-Stanford University, 1995.

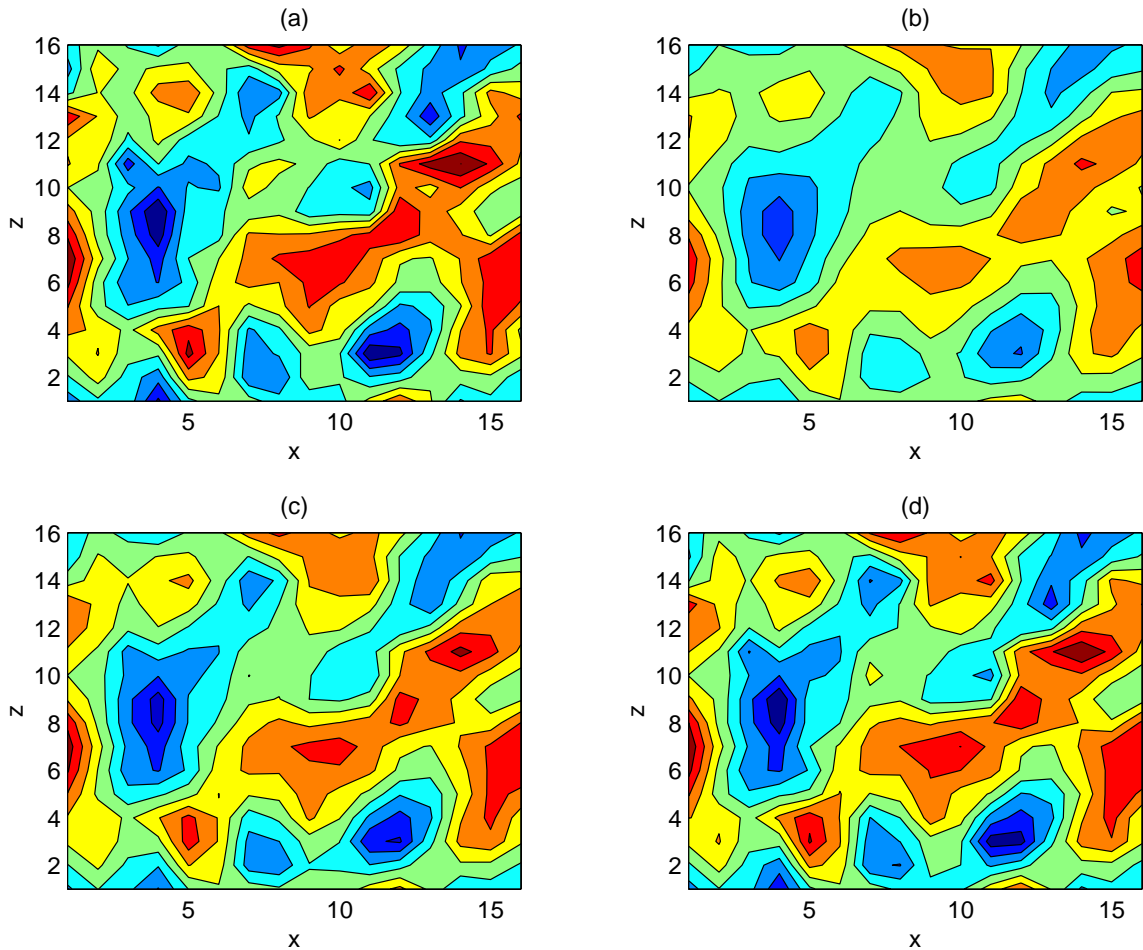


Figure 8: Contour plots of LES velocity estimates for u_1 on an x_1, x_3 -plane, $GR = 8$. (a) Sampled DNS field; (b) 2nd-order estimate; (c) 4th-order estimate; (d) 6th-order estimate.

- [11] J.A. Domaradzki and E.M. Saiki. A subgrid-scale model based on the estimation of unresolved scales of turbulence. *Physics of Fluids*, 9(7):2148–2164, 1997.
- [12] J.A. Domaradzki and K.-C. Loh. The subgrid-scale estimation model in the physical space representation. *Physics of Fluids*, 11(8):2330–2342, 1999.
- [13] B.J. Geurts. Inverse modeling for large-eddy simulation. *Physics of Fluids*, 9(12):3585–3587, 1997.
- [14] S. Stolz and N.A. Adams. An approximate deconvolution procedure for large-eddy simulation. *Physics of Fluids*, 11(7):1699–1701, 1999.
- [15] S. Liu, C. Meneveau, and J. Katz. On the properties of similarity subgrid-scale models as deduced from measurements in a turbulent jet. *Journal of Fluid Mechanics*, 275:83–119, 1994.
- [16] F.V. Katopodes, R.L. Street, and J.H. Ferziger. Subfilter-scale scalar transport for large-eddy simulation. In *14th Symposium on Boundary Layer Turbulence*, pages 472–475, 2000.

- [17] C.G. Speziale. Galilean invariance of subgrid-scale stress models in the large-eddy simulation of turbulence. *Journal of Fluid Mechanics*, 156:55–62, 1985.
- [18] K. B. Shah. *Large eddy simulations of flow past a cubic obstacle*. PhD thesis, Stanford University, 1998.
- [19] L. Ding. Personal communication, 2000.
- [20] S. Ghosal and P. Moin. The basic equations for the large eddy simulation of turbulent flows in complex geometry. *Journal of Computational Physics*, 118:24–37, 1995.
- [21] R.A. Clark, J.H. Ferziger, and W.C. Reynolds. Evaluation of subgrid-scale turbulence models using a fully simulated turbulent flow. Technical Report TF-9, Department of Mechanical Engineering, Stanford University, Stanford, California, 1977.
- [22] R.A. Clark, J.H. Ferziger, and W.C. Reynolds. Evaluation of sub-grid-scale models using an accurately simulated turbulent-flow. *Journal of Fluid Mechanics*, 91:1–16, 1979.
- [23] L.H. Shih, J.R. Koseff, J.H. Ferziger, and C.R. Rehmann. Scaling and parameterization of stratified homogeneous turbulent shear flow. *Journal of Fluid Mechanics*, 412:1–20, 2000.
- [24] S. Stolz, N.A. Adams, and L. Kleiser. Analysis of subgrid scales and subgrid scale modeling for shock-boundary-layer interaction. In *First International Symposium on Turbulence and Shear Flow Phenomena*, pages 881–886, Santa Barbara, California, 1999.
- [25] M.V. Salvetti and S. Banerjee. *A priori* tests of a new dynamic subgrid-scale model for finite-difference large-eddy simulations. *Physics of Fluids*, 7(11):2831–2847, 1995.
- [26] Y. Zang, R. L. Street, and J. R. Koseff. A non-staggered grid, fractional step method for time dependent incompressible Navier-Stokes equations in curvilinear coordinates. *Journal of Computational Physics*, 114(1):18–33, 1994.
- [27] M.V. Salvetti, Y. Zang, R.L. Street, and S. Banerjee. Large-eddy simulation of free-surface decaying turbulence with dynamic subgrid-scale models. *Physics of Fluids*, 9(8):2405–2419, 1997.